

Large-Porous Catalysts Consisting of Nanosized ZSM-5 Zeolite Crystals for *n*-Hexane Cracking Process

E. E. Vorobyeva^{a,b,*}, D. A. Sladkovskii^c, A. I. Lysikov^{a,b}, and E. V. Parkhomchuk^{a,b}

^a Boreskov Institute of Catalysis, Siberian Branch of Russian Academy of Sciences (BIC SB RAS), Novosibirsk, 630090 Russia

^b Novosibirsk State University, Novosibirsk, 630090 Russia

^c St. Petersburg State Institute of Technology (Technical University), St. Petersburg, 190013 Russia

*e-mail: catherina.vorobieva@gmail.com

Received October 19, 2020; revised November 10, 2020; accepted November 16, 2020

Abstract—The paper reports the preparation of two series of nanosized (150–350 nm) ZSM-5 zeolite crystals with a Si/Al molar ratio of 70 to 144 by a template method. The prepared catalysts are distinctive in their mostly intercrystalline macroporosity and random architecture of transport channels formed as a result of the utilization of a high-molecular-weight template represented by suspended or powdered polystyrene particles about 250 nm in size. The crystallinity and the size and packing of the particles depend on the method of template introduction into a precursor mixture. The samples of both series were tested in an *n*-hexane cracking reaction, and the comparative assessment of their catalytic properties in terms of *n*-hexane conversion degree and selectivity for alkane, olefin, and isoalkane products is also summarized in the paper.

Keywords: ZSM-5, cracking, polystyrene, *n*-hexane

DOI: 10.1134/S0965544121030014

Zeolites are widely used in industrial processes as heterogeneous acid catalysts [1]. Catalytic cracking of hydrocarbons to produce light olefins is the most significant of such processes. Light olefins are the most important raw materials for the chemical industry; they are commonly produced by the thermal cracking of naphtha. However, this process has a number of disadvantages: high temperature (800°C), selectivity that is difficult to control, low propylene/ethylene ratio in the products, and high cost. Catalytic cracking decreases process temperature to 550–650°C and increases propylene/ethylene ratio [2]. Such a process requires a highly efficient selective catalyst to be utilized. Various catalysts are most commonly tested on a model reaction of *n*-hexane cracking, because naphtha primarily contains C_{5–8} *n*-paraffins [3].

Among zeolite catalysts, ZSM-5 is of particular interest because of its advantageous properties, such as high concentration of strong acid sites, shape selectivity, ion exchange properties, and high thermal stability [4]. A variety of processes, such as protolytic cracking, thermal cracking, dehydrogenation, β-decomposition, oligomerization, cyclization, coking, and hydride

transfer, are known to occur in zeolite pores [5]. On the other hand, a major disadvantage of zeolites is their micropore size, which hinders the mass transfer of variously-sized molecules to and from the active sites. As a consequence, large molecules can only be transformed on external active sites, while small molecules can only access a limited part of a zeolite crystal [6]. In addition, the poor mass transfer of reaction products from the catalyst surface reduces its lifetime. The mass transfer efficiency can be improved by reducing the crystal size (through producing either nanocrystalline or nanolayered zeolites) or by creating a developed texture, i.e., increasing the effective diffusion coefficient [7]. Crystal size is changed by varying the hydrothermal synthesis parameters, while a number of techniques described in [8] are used to create an improved texture or hierarchy. The most attractive of such techniques is a template synthesis method. This allows one to control strictly the textural parameters of the catalyst, such as the size of meso- and macropores, the proportion of coarse pores, etc. [2]. Researchers still continue studying the catalytic cracking of *n*-hexane, since the catalyst activity results in this process are representative enough to predict the

activity in more complex processes [9]. This reaction may occur according to a monomolecular or bimolecular mechanism depending on reaction products. For example, the monomolecular mechanism primarily yields ethylene and propylene. While the bimolecular mechanism tends to promote the formation of saturated hydrocarbons [10]. The mechanism's contribution is generally estimated by the hydride anion transfer index (*HT*):

$$HT = \frac{S_{C_3H_8} + S_{n-C_4H_{10}}}{S_{C_3H_6}}$$

where *S* is the respective product selectivity.

The effects of the texture hierarchy and acidity of highly crystallized ZSM-5 zeolites with different Si/Al molar ratios and crystal sizes have been investigated earlier [2]. The most significant parameters of ZSM-5 for an *n*-hexane cracking reaction were concluded to be strong acidic site concentration and pore hierarchy factor. According to the data obtained, the maximum conversion is observed for a sample with optimum acidity and hierarchy factor.

The study reported in the paper consisted in the testing of two series of ZSM-5 crystals in *n*-hexane cracking reaction. Two series of ZSM-5 are randomly arranged nanosized crystals synthesized with a high-molecular-weight template and having various surface acidity. Also the comparison of catalytic properties of the samples in terms of *n*-hexane conversion degree and reaction rates of protolytic cracking, dehydrogenation, hydride transfer, and oligomerization was performed. The study was characterized by applying of two methods to produce nanosized zeolite crystals packed in large-porous structures with random architecture of transport channels. In both cases, large-pores were formed by adding a high-molecular-weight template into a precursor mixture. The template used consisted of suspended or powdered polystyrene particles about 250 nm in size.

EXPERIMENTAL

The following reagents were used: tetraethyl orthosilicate (TEOS, from Angara-Reaktiv), tetrapropyl ammonium hydroxide (TPAOH, 25 wt % aqueous solution, from Acros), ethanol (EtOH), aluminum isopropoxide [Al(OPr-*i*)₃, from Acros], distilled water for zeolite synthesis, aqueous ammonia (NH₄OH, AR grade, from Chemical Depot no. 1) for zeolite treatment, as well as styrene (from Angara-Reaktiv), ammonium persulfate (CP grade, from Reachem), and nitrogen to prepare a high-molecular-weight template.

A catalyst template in the form of polymeric microspheres was prepared by emulsion polymerization according to the method described in [11]. Prior to the synthesis, styrene was washed to remove inhibitors in a separation funnel with a 0.1 M NaOH solution until discoloration was completed, followed by water washing to reach neutral pH. Then 3.2 L of nitrogen-bubbled water was thermostated in a reactor at 90°C. Next, 0.16 L of styrene and, 10 min later, 2 g of an ammonium persulfate initiator dissolved in 50 mL of water, were added to the reactor. The synthesis was held for 24 h with a stirring rate of 400 rpm. The resulting particle size was monitored on a Photocor Compact-Z instrument with the following laser parameters: $\lambda = 638$ nm; $P = 25$ mW. The prepared template had a concentration of 0.050 ± 0.005 g/mL. The suspension was evaporated at 50°C when required.

Zeolite samples were synthesized under hydrothermal conditions in the presence of TPAOH. TEOS was used as a silicon source and Al(OPr-*i*)₃ as an aluminum source. The synthesis procedure consisted of the following sequence. The required amount of Al(OPr-*i*)₃ was stirred in 2 mL of TPAOH (Solution I) until complete dissolution. 10 mL of TEOS was added to 10 mL of H₂O and 18 mL of TPAOH (Solution II) and stirred for 24 h. 10 mL of ethanol was added to Solution II and stirred. Solution I was added dropwise to Solution II. 40 mL of the polystyrene template (PS template) was added for the ST-series, and 2 g of the powdered template was added for the T-series, and stirred for 1 h. The synthesis was run in an autoclave with a teflon cup at 90°C for 240 h. After cooling of the autoclaves, the prepared suspensions were centrifuged, and the precipitate was washed with distilled water to neutral pH. The washed precipitate was dried at 50°C for 24 h. The samples were calcined at 550°C for 5 h at a heating rate of 2 deg/min. The synthesis data are summarized in Table 1. The zeolite yield and crystallinity are presented in Table 2.

The total zeolite yield was calculated as a weight ratio between the obtained calcined solid and the total of SiO₂ and Al₂O₃ in the initial mixture. The sample's relative crystallinity was derived from the area of reflections on the X-ray diffraction pattern in the angle range of 22°–25° with respect to the most crystallized sample of the respective series.

X-ray diffraction analysis (XRD) of 0.17 g samples was carried out on a Siemens D500 diffractometer, where

Table 1. Synthesis summary

Sample	Estimated Si : Al molar ratio	PS template form	Molar ratio between components
ST-100	100	Suspension	1SiO ₂ : 0.005Al ₂ O ₃ : 0.5TPAOH : 3.5EtOH : 12H ₂ O
ST-200	200		1SiO ₂ : 0.0025Al ₂ O ₃ : 0.5TPAOH : 3.5EtOH : 12H ₂ O
ST-300	300		1SiO ₂ : 0.0017Al ₂ O ₃ : 0.5TPAOH : 3.5EtOH : 12H ₂ O
T-100	100	Powder	1SiO ₂ : 0.005Al ₂ O ₃ : 0.5TPAOH : 3.5EtOH
T-200	200		1SiO ₂ : 0.0025Al ₂ O ₃ : 0.5TPAOH : 3.5EtOH
T-300	300		1SiO ₂ : 0.0017Al ₂ O ₃ : 0.5TPAOH : 3.5EtOH

Table 2. Component ratios for synthesis of ZSM-5 samples with various Si/Al ratio and crystal size, product yield, and relative crystallinity

Sample	Estimated Si : Al molar ratio	Experimental Si : Al molar ratio	Zeolite yield, %	Crystallinity, %
ST-series				
ST-100	100	70	18	97
ST-200	200	141	29	100
ST-300	300	144	41	99
T-series				
T-100	100	79	20	76
T-200	200	126	34	58
T-300	300	139	42	76

monochromatized CuK_α radiation ($\lambda = 1.54 \text{ \AA}$) was used to record the spectra.

The scanning electron microscopy (SEM) images were obtained on a JEOL JSM-6460LV instrument at an accelerating voltage of 15–20 kV.

The zeolite porous structure was determined by low-temperature nitrogen porometry. The nitrogen adsorption/desorption isotherms at 77 K were measured using a Quadrasorb EVO specific surface and porosity analyzer manufactured by Quantachrome Instruments (USA). To remove adsorbed gases and moisture, all the samples were degassed in a vacuum at 300°C for 10 h. The specific surface was calculated by a BET equation, in accordance with the IUPAC recommendations and using a direct method for computing the BET equation parameters to eliminate errors arising from the capillary condensation effect in narrow mesopores. The pore size distribution was determined by an NLDFT statistical mechanics method using a model of nitrogen adsorption in cylindrical silica pores at 77 K. The calculation was performed in the software supplied with the instrument.

The hierarchy factor (*HF*) was estimated by the following formula [2]:

$$HF = \frac{V_{\mu}}{V_{\Sigma}} \cdot \frac{S_{\text{ext}}}{S_{\text{BET}}},$$

where V_{μ} is the micropore specific volume; V_{Σ} is the total pore specific volume, S_{ext} is the external specific surface area, and S_{BET} is the specific surface area.

The acidity was measured by temperature-programmed desorption of ammonia (NH₃-TPD) in a series of steps in a semi-automatic mode. The acidity was determined as the NH₃ adsorption capacity of the samples; the amount of NH₃ adsorbed on the acid sites of different strengths was derived from the peak areas with maxima at T_{max} obtained through approximating the NH₃-TPD curves to a set of Gaussian peaks. The samples were analyzed after the catalysts had been tested in the *n*-hexane cracking reaction for 30 min and calcined at 550°C for 5 h at a heating rate of 2 deg/min. The ST-100 acidity is presented for the sample newly calcined under the same conditions.

The silicon and aluminum weight contents were determined by inductively coupled plasma atomic emission spectrometry (ICP-AES) on a Baird (Holland) instrument. The samples were preliminarily acid-dissolved in an HNO₃/HF mixture in a MARS-6 microwave system under heating conditions (180°C for 20 min and 200°C for 20 min).

The zeolite tests in an *n*-hexane cracking reaction were carried out similarly to the method described in [9] at 450°C and atmospheric pressure in a flow-through reactor with 1 g of catalyst load. A catalyst particle size of 140–500 μm mesh was obtained by molding and grinding a zeolite powder with screening through 0.14 mm and 0.5 mm sieves. The feedstock was introduced with a dried *n*-hexane-saturated helium stream by gas bubbling through a liquid *n*-hexane layer. The feed weight hourly space

velocity (WHSV) corresponded to $0.86 \text{ g}_{n\text{-hexane}}/(\text{g}_{\text{cat}} \text{ h})$. The reaction products were collected in a gasometer and analyzed every 30 min with emptying upon each sampling. Prior to the experiment, the catalyst was activated (dehumidified) by dry helium purging at 450°C for 1 h. Both the feedstock and the products were analyzed on a Shimadzu GC-2010 Plus gas chromatograph equipped with a FID and a Supelco Petrocol DH $100 \text{ m} \times 0.25 \text{ mm}$ capillary column (polydimethyl siloxane). The chromatograms were processed in Dragon DHA software using a reference sample of $\text{C}_1\text{--C}_7$ hydrocarbons produced from n -hexane cracking.

The n -hexane conversion was determined by the formula:

$$X = (C_{nC_6}^{\text{in}} - C_{nC_6}^{\text{out}}) / C_{nC_6}^{\text{in}},$$

where $C_{nC_6}^{\text{in/out}}$ is the n -hexane weight content at the reactor inlet/outlet.

The product selectivity was determined by the formulas:

$$n_i = (GC_i^{\text{out}} - GC_i^{\text{in}}) / M_i, \\ S_i = n_i / (\sum n_i),$$

where $C_i^{\text{in/out}}$ is the weight content of the i th component at the reactor inlet/outlet; G (g/h) is the hydrocarbon WHSV to the reactor; n_i (mol/h) is the quantity of the i th reaction product; and M_i (g/mol) is the molar mass of the i th product.

The method presented in [9] was used to estimate the reaction pathways. The protolytic cracking reaction rate (r_{PC}) was derived from the sum of $\text{C}_1\text{--C}_4$ n -alkane selectivities (S_{PC}) by the formula:

$$r_{\text{PC}} = \text{WHSV} \cdot X \cdot S_{\text{PC}} / M_w, \\ S_{\text{PC}} = S_{\text{CH}_4} + S_{\text{C}_2\text{H}_6} + S_{\text{C}_3\text{H}_8} + S_{n\text{-C}_4\text{H}_{10}},$$

where WHSV (g/g-s) is the weight hourly space velocity of the n -hexane feed; and M_w (g/mol) is the n -hexane molar mass.

The dehydrogenation reaction rate (r_{DEH}) was derived from the total $\text{C}_2\text{--C}_6$ olefin selectivity (S_{olef}) less the cracking selectivity, because protolytic cracking is assumed to produce 1 mole of olefin per mole of an n -alkane product. Thus, the balance amount of olefins is formed in the dehydrogenation reactions of n -hexane and cracking products:

$$r_{\text{DEH}} = \text{WHSV} \cdot X (S_{\text{olef}} - S_{\text{PC}}) / M_w, \\ S_{\text{olef}} = S_{\text{C}_2\text{H}_4} + S_{\text{C}_3\text{H}_6} + S_{\text{C}_4\text{H}_8} + S_{\text{C}_5\text{H}_{10}} + S_{\text{C}_6\text{H}_{12}}.$$

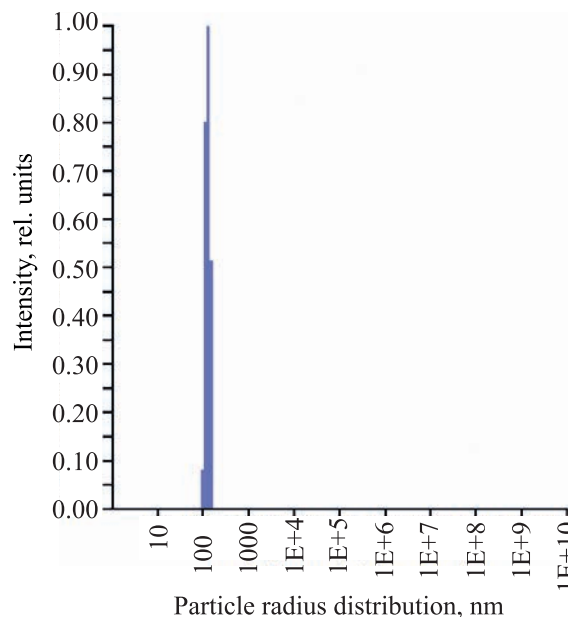


Fig. 1. Dynamic light scattering for the synthesized template.

The hydride ion transfer reaction rate (r_{HT}) was calculated based on the isoalkane selectivities:

$$r_{\text{HT}} = \text{WHSV} \cdot X (S_{i\text{-C}_4\text{H}_{10}} + S_{i\text{-C}_5\text{H}_{12}} + S_{i\text{-C}_6\text{H}_{14}}) / M_w.$$

RESULTS AND DISCUSSION

According to dynamic light scattering data obtained for the synthesized template (Fig. 1), polystyrene microspheres have a monomodal particle size distribution with a maximum at 125 nm, which corresponds to a diameter of about 250 nm. The concentration of the template used was, on average, $0.050 \pm 0.005 \text{ g/mL}$.

Figure 2 demonstrates the XRD patterns of the samples from both the ST- and T-series, where a high-molecular-weight template in the form of suspension and dry powder, respectively, was used for the synthesis. These samples consist of randomly arranged particles 120 to 350 nm in size. The two series are different in the size and arrangement of the crystals. The ST-series crystal size ranges between 250 and 350 nm, while the T-series varies from 150 nm or even finer crystals to 250 nm. The XRD reveals that the samples in both series are represented by MFI type zeolites, where the ST-series samples have an appreciably higher crystallinity than the T-series (Table 2, Fig. 2). In all probability, the addition of a dry powdered template consisting of aggregated hydrophobic polystyrene microspheres leads to a more significant layering of the precursor mixture than in the case of polymer solution with monodisperse particles.

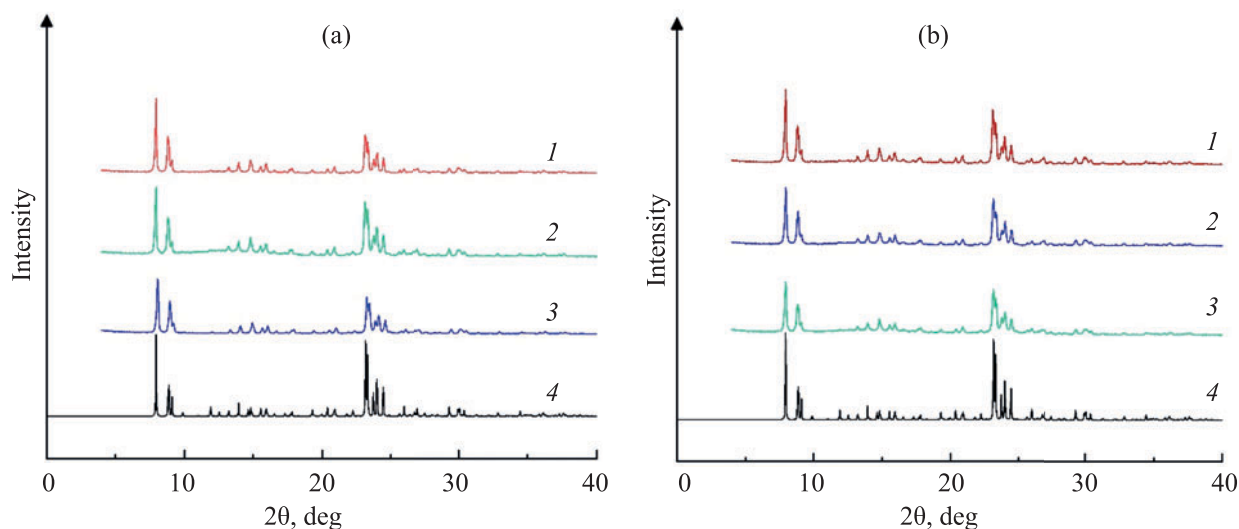


Fig. 2. XRD patterns of both series. (a): (1) ST-300, (2) ST-200, (3) ST-100, (4) MFI and (b): (1) T-300, (2) T-200, (3) T-100, (4) MFI.

This addition also appears to form a zone with higher TEOS concentration and lower water content in the aggregate pores, where zeolite crystallization occurs, as well as a zone with higher concentration of water-soluble components, including TPAOH. With such layering,

the resulting T-series samples contain finer crystals and exhibit a higher fraction of an amorphous phase or a phase consisting of 20 nm and finer particles, than the ST-series samples. A similar regularity with a crystallinity decline and with the formation of appreciably finer crystals was observed in a prior study where synthesis in the presence of polymeric microspheres was used instead of traditional hydrothermal synthesis [12].

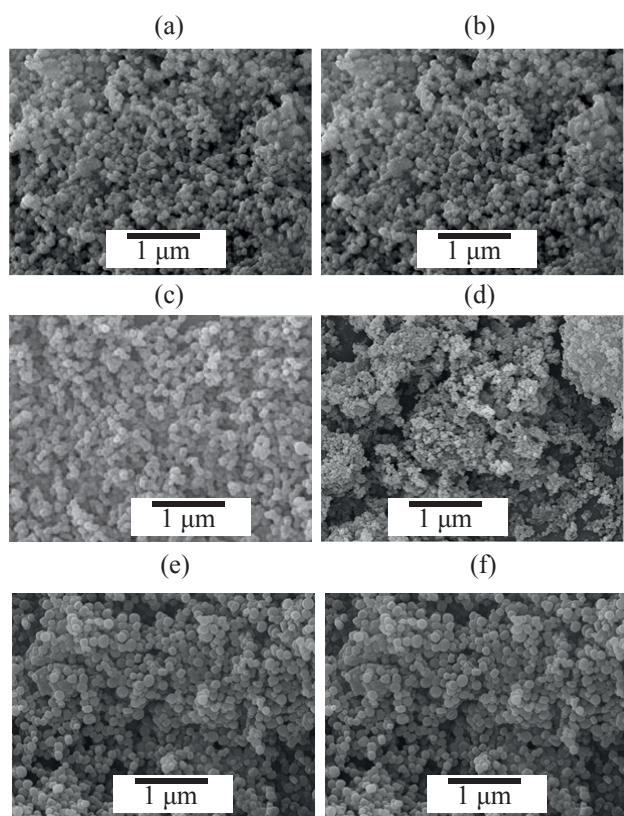


Fig. 3. SEM images of both series. (a) ST-100, (b) T-100, (c) ST-200, (d) T-200, (e) ST-300, (f) T-300.

The addition of a high-molecular-weight template, suspended or dry powdered, creates a different packing architecture of zeolite crystals because the template serves as a matrix in which crystals grow. At the specified zeolite synthesis temperature (90°C), the polystyrene microspheres do not melt. Moreover, at high pH, the negative charge of the particles prevents them from aggregation. Therefore, a suspended template is represented by individual microspheres on which TEOS hydrolysis occurs with subsequent growth in the size of zeolite nanocrystals. However, a dry powdered polymeric template is a colloidal crystal the particles of which are unlikely to be completely dispersed into individual microspheres; moreover, the solution may be segregated into an organic layer and an aqueous layer to form finer crystals in the porous space of the template aggregate. When the matrix is removed, a framework of differently packed nanocrystals remains. As such, the ST series exhibits more homogeneous architecture of nanocrystal packing, where the particles form ~200 nm channel walls. The T-series SEM images (Fig. 3) indicate that the powdered template acts as a non-homogeneous matrix. As it turns out, finer zeolite particles form channels of

Table 3. Textural and acid properties of ZSM-5 samples

Sample	S_{BET} , m ² /g	S_{ext} , m ² /g	V_{micro} , cm ³ /g	V_{meso} , cm ³ /g	V_{macro} , cm ³ /g	Hierarchy factor	$a_{\text{m}}(\text{NH}_3)$, mmol/g	T_{max} , °C	$n(\text{NH}_3)$, mmol/g
ST-series									
ST-100	582	206	0.13	0.1	0.36	0.08	0.29	183	0.076
								231	0.090
								444	0.122
ST-200	527	166	0.14	0.07	0.29	0.09	0.23	162	0.078
								218	0.092
								464	0.055
ST-300	482	118	0.13	0.04	0.25	0.08	0.16	161	0.070
								210	0.065
								447	0.023
T-series									
T-100	517	221	0.12	0.2	0.42	0.07	0.27	150	0.101
								206	0.132
								427	0.097
T-200	499	173	0.13	0.18	0.35	0.07	0.20	153	0.076
								209	0.094
								439	0.060
T-300	505	196	0.12	0.21	0.29	0.08	0.19	158	0.072
								209	0.077
								443	0.044

various sizes, from hundreds of nanometers to several microns.

According to the BET data (Table 3), the samples have micro/macro-porous texture. The nitrogen adsorption isotherms of both ZSM-5 series at 77 K are basically similar in pattern to the IUPAC Type I isotherms (Fig. 4) typical of micro-porous samples [13]. It is worth noting

that the samples of both series have approximately the same micropore volume, specifically about 0.13 cm³/g. This implies that the lower crystallinity of T-series results from the large fraction of the phase with fine zeolite nanocrystals, which have a MFI structure despite the absence of the corresponding XRD pattern reflections. At P/P_0 of 0.8 to 1.0, hysteresis appears due to the

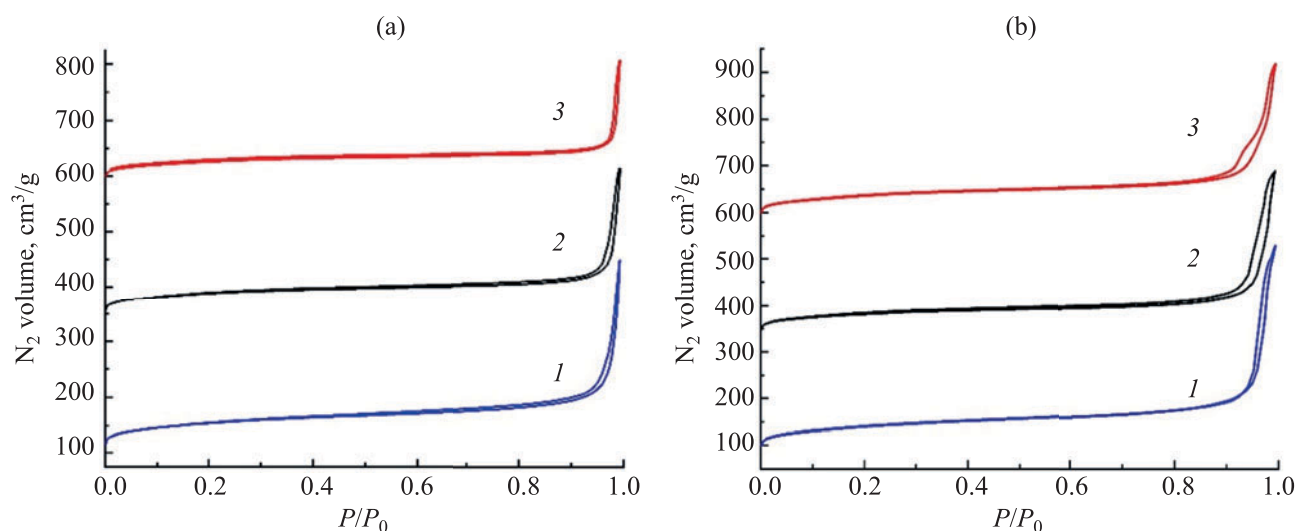


Fig. 4. Nitrogen adsorption isotherms of both series. (a): (1) ST-300, (2) ST-200, (3) ST-100 and (b): (1) T-300, (2) T-200, (3) T-100. For illustrative purposes, the isotherms are shifted by 250 cm³/g with respect to one another along the Y-axis.

Table 4. Catalytic test summary

Catalyst	ST-100	ST- 200	ST-300	T-100	T-200	T-300
Run parameters						
Hexane conversion degree, %	28.1	63.6	33.3	48.7	28.8	19.6
Total C ₁ –C ₄ <i>n</i> -alkanes, %	45.2	57.6	43.5	53.3	52.9	49.3
Total C ₁ –C ₅ olefins, %	50.0	34.9	46.0	38.8	28.5	34.6
Olefins/ <i>n</i> -alkanes	1.1	0.6	1.1	0.7	0.5	0.7
Hydride anion transfer index	1.3	3.3	1.5	2.4	3.7	2.6
Reaction rate, mol/(g s)×10 ⁹						
Protolytic cracking	233.3	671.3	264.7	473.3	271.1	174.3
C ₁ –C ₅ dehydrogenation	27.9	0	20.4	0	0	0
Hydride transfer	18.4	85.0	63.3	65.2	104.7	57.7
Oligomerization	7.0	12.0	5.3	11.6	4.7	3.3
Component selectivity, mol %						
C₁–C₄ gases	97.1	97.2	95.1	96.4	91.4	91.1
Methane	5.7	4.0	14.9	3.6	0.6	1.2
Ethylene	16.2	14.1	21.7	13.9	6.7	8.3
Ethane	7.4	6.1	4.6	5.9	1.8	3.6
Propylene	25.2	14.1	15.5	17.6	13.1	16.5
Propane	26.5	39.0	17.7	35.1	35.7	34.3
Isobutene	2.4	5.6	6.4	5.3	12.3	8.6
<i>n</i> -Butane	5.2	7.6	5.4	7.7	12.4	8.8
C ₄ butenes	8.6	6.6	8.8	7.3	8.6	9.8
Total C₅	0.9	1.6	1.9	1.8	4.4	2.7
Isopentane	0.3	0.8	1.1	0.9	2.1	1.3
<i>n</i> -Pentane	0.6	0.8	0.9	0.9	2.3	1.4
Cyclopentane	0.0	0.0	0.0	0.0	0.0	0.0
C ₅ olefins	0.0	0.0	0.0	0.0	0.0	0.0
Total C₆	0.7	0.1	2.1	0.5	3.4	5.4
2,2-Dimethyl butane	0.0	0.0	0.0	0.0	0.0	0.1
2,3-Dimethyl butane	0.0	0.0	0.2	0.0	0.2	0.4
3-Methyl pentane	0.2	0.0	0.8	0.0	1.2	2.0
2-Methyl pentane	0.1	0.0	0.8	0.0	1.4	2.1
<i>n</i> -Hexane	0.0	0.0	0.0	0.0	0.0	0.0
MCP+CH	0.4	0.1	0.3	0.4	0.5	0.7
C ₆ olefins	0.0	0.0	0.0	0.0	0.0	0.0
Total C₇₊	1.3	1.0	0.9	1.3	0.9	0.9

presence of macropores formed through the aggregation of nanocrystals and the formation of intercrystalline pores. All the samples of both series exhibit high specific surface and external surface areas and high pore volumes; the pore hierarchy factor ranges between 0.07 and 0.09 and demonstrates the large contribution of large intercrystalline meso- and macropores and the small proportion of intracrystalline mesopores. The T-series has a larger mesopore volume than the ST-series, which may be associated with the more random packing and the aggregation of finer crystals.

The assessment of the NH₃-TPD curves showed (Table 3, Fig. 5) the predictable acidity decline with an increase in Si/Al molar ratio in both series.

Among all the samples, the maximum *n*-hexane conversion (63.6%) is achieved in ST-200, 48.7% in T-100, and about 30% in ST-100, T-200, and ST-300. The minimum conversion (19.6%) corresponds to T-300 (Table 4). High olefin selectivity (50.0% and 46.0%) is observed in ST-100 and ST-300, respectively. As such, ST-100 exhibits the highest propylene selectivity (25.2%), while ST-300 has the best ethylene selectivity (21.7%), which also influences dehydrogenation rate. The lowest

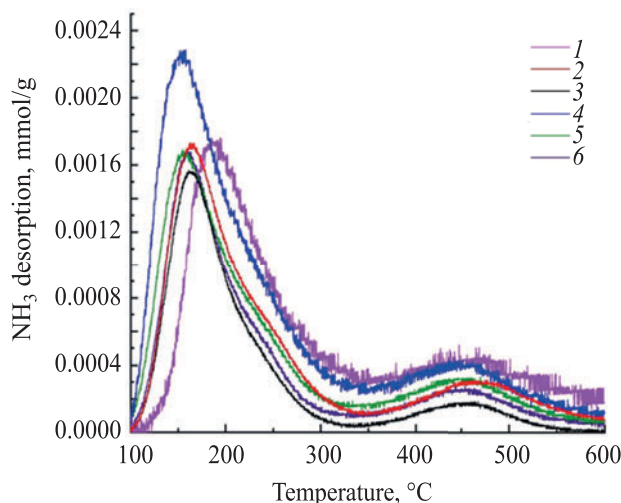


Fig. 5. NH₃-TPD curves of zeolite samples: (1) ST-300, (2) ST-200, (3) ST-100, (4) T-300, (5) T-200, (6) T-100.

hydride anion transfer index is in ST-100, the sample, from among all samples of both series, with the highest aluminum content and high acidity. This indicates the highest contribution of the monomolecular cracking mechanism in this sample. In general, the other samples have a propylene selectivity of about 15% and an ethylene selectivity of about 15%, except for T-200 (6.7%) and T-300 (8.3%).

CONCLUSIONS

The analysis of the two ZSM-5 series demonstrates that the hydrothermal synthesis of the ST-series samples, in which the polymeric template consisting of monodisperse microspheres was uniformly distributed across the precursor mixture, produces a homogeneous micro/macro-porous large-nanocrystalline structure. Similar synthesis of the T-series samples, with the addition of colloidal crystals of the same polymeric microspheres, forms finer nanocrystals packed in a non-homogeneous structure. Despite the substantially higher crystallinity of the ST-series, the samples of both series have the same specific micropore volume, which may evidence the same fraction of MFI phase and a larger contribution of fine nanocrystals in the T-series. The presence of this X-ray-amorphous phase, which has a specific micropore volume corresponding to the MFI phase, is assumed to be undesirable for the *n*-hexane cracking reaction. Thus, it leads to the significantly larger contribution of the bimolecular mechanism for the T-series than for ST. The highest propylene selectivity in *n*-hexane cracking is observed in the presence of ST-100, which possesses a homogeneous micro/macro-porous structure with 250–

350 nm nanocrystalline walls and exhibits the highest aluminum content and the highest acidity among all the samples of both series.

AUTHOR INFORMATION

E.E. Vorobyeva, ORCID: <https://orcid.org/0000-0002-7435-9740>

D.A. Sladkovskii, ORCID: <https://orcid.org/0000-0002-1231-802X>

A.I. Lysikov, ORCID: <https://orcid.org/0000-0003-3998-7204>

E.V. Parkhomchuk, ORCID: <https://orcid.org/0000-0003-2200-884X>

ACKNOWLEDGMENTS

The reported study was performed within the framework of the state assignment for BIC SB RAS. The authors are grateful to the following researchers of BIC SB RAS: T.A. Alekseeva for conducting XRD, N.A. Rudina for recording SEM images, A.A. Leonova for conducting textural experiments, and A.A. Pochtar for chemical analysis of the samples.

CONFLICT OF INTEREST

The authors declare no conflict of interest requiring disclosure in this article.

REFERENCES

1. Vermeiren, W. and Gilson, J.P., *Top. Catal.*, 2009, vol. 52, no. 9, p. 1131. <https://doi.org/10.1007/s11244-009-9271-8>
2. Parkhomchuk, E., Sladkovskii, D., Gun, Y., Wu, W., Sashkina, K., Lysikov, A., and Parmon, V., *Pet. Chem.*, 2019, vol. 59, no. 3, p. 338. <https://doi.org/10.1134/S0965544119030113>
3. Kubo, K., Iida, H., Namba, S., and Igarashi, A., *J. Japan Petrol. Inst.*, 2018, vol. 61, no. 1, p. 10. <https://doi.org/10.1627/jpi.61.10>
4. Rahimi, N. and Karimzadeh, R., *Appl. Catal. A: General*, 2011, vol. 398, nos. 1–2, p. 1. <https://doi.org/10.1134/S0965544119030113>
5. Vogt, E., Whiting, A., Dutta Chowdhury, A., and Weckhuysen, B., *Adv. Catal.*, 2015, vol. 58, p. 143. <https://doi.org/10.1016/bs.acat.2015.10.001>
6. Feliczak-Guzik, A., *Micropor. Mesopor. Mater.*, 2018, vol. 259, p. 33. <https://doi.org/10.1016/bs.acat.2015.10.001>
7. Hartmann, M., Machoke, A.G., and Schwieger, W., *Chem. Soc. Rev. Royal Society of Chemistry*, 2016, vol. 45, no. 12, p. 3313. <https://doi.org/10.1039/c5cs00935a>
8. Schwieger, W., Machoke, A., Weissenberger, T., Inayat, A., Selvam, T., Klumpp, M., and Inayat, A.,

- Chem. Soc. Rev. Royal Society of Chemistry*, 2016, vol. 45, no. 12, p. 3353.
<https://doi.org/10.1039/C5CS00599J>
9. Brait, A., Seshan, K., and Lercher, J.A., *Appl. Catal. A: General*, 1998, vol. 169, no. 2, p. 299.
[https://doi.org/10.1016/S0926-860X\(98\)00023-4](https://doi.org/10.1016/S0926-860X(98)00023-4)
 10. Corma, A. and Orchillés, A.V., *Micropor. Mesopor. Mater.*, 2000, vols. 35–36, p. 21.
[https://doi.org/10.1016/S0021-9517\(02\)00132-X](https://doi.org/10.1016/S0021-9517(02)00132-X)
 11. Zou, D., Ma, S., Guan, R., Park, M., Sun, L., Aklonis, J., and Salovey, R., *J. Polym. Sci. Part A Polym. Chem.*, 1992, vol. 30, no. 1, p. 137.
<https://doi.org/10.1002/pola.1992.080300118>
 12. Parkhomchuk, E., Sashkina, K., and Parmon, V., *Pet. Chem.*, 2016, vol. 56, no. 3, p. 197.
<https://doi.org/10.1134/S0965544116030105>
 13. Thommes, M., Kaneko, K., Neimark, A., Olivier, J., Rodriguez-Reinoso, F., Rouquerol, J., and Sing, K., *Pure Appl. Chem.*, 2015, vol. 87, nos. 9–10, p. 1051.
<https://doi.org/10.1515/pac-2014-1117>